aerospace

MDPI

Article

Use of Unconventional Laminates for the Design of a Buckling-Driven Twisting Composite Wing Box

Anatoli Mitrou and Chiara Bisagni *

Department of Aerospace Science and Technology, Politecnico di Milano, Via La Masa 34, 20156 Milan, Italy; anatoli.mitrou@polimi.it

* Correspondence: chiara.bisagni@polimi.it

Abstract

The inherent directionality in the behavior of composite laminates in conjunction with buckling can be used to develop adaptive composite structures. In this direction, this study focuses on optimizing the bending–twisting coupling response of a composite wing box in a simplified representation. Focus is given to the potential benefits of the use of both standard and unconventional laminates to achieve this. The designs are obtained utilizing a particle swarm optimization (PSO) algorithm based optimization framework. The results demonstrate that while the optimal solution is one that arises from the use of standard ply angles, i.e., typical quads, solutions relying on a combination of unconventional lay-ups produce similar levels of twisting while remaining more versatile, also leading to an achievable multi-stable design.

Keywords: adaptive structures; buckling; composites; non-standard angle laminates; particle swarm optimization

1. Introduction

As is understood, aircraft wings are, in fact, flexible structures and their flexibility is a desired characteristic. Indeed, it is common to want them to adjust their shape depending on certain stimuli, e.g., external loads. This has been common practice for years and has been studied through the use of many innovative technologies often referred to as morphing or adaptive capabilities [1–16]. In this vast field of adaptive technologies and capabilities, there is a subset that deals with the specific case of bending–twisting coupling of the response of wings and winglike structures for matters of either load alleviation or overall drag reduction affecting the overall efficiency of the structure [3,4,7,10,15,17–21].

Considering the structure itself, if one were to consider undertaking this task using traditional metallic materials, it is unlikely they would render any impressive results. In fact, many of these technologies rely on utilizing fiber-reinforced composite materials, which are characterized by inherent anisotropy and directionality, and potentially strong elastic couplings that can however be tailored. Fairly recently, in this realm, some works focused specifically on tuning the response of wing structures considering an inherent material mechanical response, buckling. Given that this instability inevitably reduces the structure's stiffness, it has, thus far, mainly been avoided. However, designing towards a direction of utilizing it instead of avoiding it can be rather interesting, both in primary and secondary structures. In fact, it could also allow for a rather more passive, meaning not reliant on actuators or other mechanical members, adaptability of wings [4,6,7,11,16].

Check for updates

Academic Editor: Morteza Abouhamzeh

Received: 16 July 2026
Revised: 14 August 2026
Accepted: 20 August 2026
Published: 25 August 2026

Copyright: © 2026 by the authors. Licensee MDPI, Basel, Switzerland. This article is an open access article distributed under the terms and conditions of the Creative Commons Attribution (CC BY) license.

Among those works, there are a couple of prominent ones that specifically focus on the use of spanwise buckling of composite wings, namely the buckling of the spars of the wing, to induce twisting of the wing under bending. Runkel et al. [7] numerically studied a representative wing, containing a composite wing box, made of a combination of thick $[0_6, \pm 45]$s carbon fiber-reinforced polymer (CFRP) composite laminates and a unidirectional (UD) laminate for the rear spar, acting as the buckling member. With this configuration, they were able to reach a maximum of 2.5° rotation at the free edge, as stated due to the buckling alone. One of the main objectives of the work was to qualitatively assess the effect the fiber angle of the UD web would have on the response, meaning stiffness reduction after buckling and eventual twisting of the edge. What is interesting to note is that the wing box is overall characterized by elastic asymmetry, since the buckling web is a UD laminate differing in terms of elasticity, with respect to the other webs, alongside geometric asymmetry, since the UD web was designed to be from approximately five to thirteen times thinner that the rest of the webs (maximum twisting was reported for the latter case), that even in the pre buckling regime would lead to a level of rotation that is translated into the post buckling regime.

Zhang and Bisagni [4] studied the post-buckling response of a composite wing box, hollow rectangular beam with all webs made of quasi-isotropic (QI) CFRP laminates; however, with one of the spars being three times thinner than the rest. The main objective of the study was to investigate the effects of constraint mechanisms in the post-buckling regime and how stiffness could be altered to tailor the stiffness reduction and eventual twisting of the free edge. The work provided a good basis for understanding the phenomena linked to such design of composite wing boxes, since other loading conditions, apart from bending, were also considered. Indeed, what one can deduce from this study is that it also provides a direct understanding of the response purely due to the thickness inhomogeneity since the buckling web itself is QI like the rest of the webs, providing the box beam with an overall symmetry in terms of elasticity but not geometry.

Along those lines, but in an effort to decouple the problem from geometrical effects, and considering the cases already studied, a decision was made to focus on trying to see how and if the elasticity of the composite laminates alone can suffice to design a buckling induced adaptive composite wing box. This is linked to studying how unconventional lamination can benefit the design of a composite wing box by enabling towards a tailored and optimized bending–twisting response driven by buckling in the spanwise direction. It is noted that the classification of unconventional laminates, in this work, pertains to the use of non-standard angles in the laminate lay-ups, namely, the angles vary from the more typically used quads 0°, 90°, ±45°. It is noted that the angles of ±30° and ±60°, used in a QI laminate arrangement, are also considered standard and the respective laminate a standard laminate. Any other angle in the −90–90° range is considered a non-standard angle and the resulting laminate from combinations of those angles for its lay-up an unconventional laminate.

It is emphasized that this study's objective was not to provide an actual wing design but rather to focus on studying the mechanics and how lamination could affect the overall response of a composite box beam under bending and twisting in the post-buckling regime. In what follows, the procedure developed to define standard angle and unconventional angle laminates to study the response of a simplified representation of a wing box is elaborated. Following that, the obtained designs are compared with each other, and a discussion follows on their relevance, applicability and positive and negative aspects.

2. Problem Definition and Methodology

As stated, the problem under study is the bending–twisting coupling of a composite wing box. The idea is to try to quantify and qualitatively assess potential twisting that can be achieved in a fully composite wing box driven by buckling of one or more of the components of said wing box. The driving mechanism in this work is considered to be the buckling of the spars. Specifically, what is studied is the response under bending when one spar undergoes buckling, which, at that point and in the post-buckling phase, induces twisting due to a shift in the spar stiffness which creates a sort of torsional movement.

As shown in Figure 1, the idea departs from a simplified representation of a wing which considers a main wing box, consisting of just the spars, ribs and the skin. The wing box intersects the wing between the leading edge and the trailing edge. In terms of kinematics, it is considered that the leading and trailing edges will follow the wing box with a rigid body type motion and are thus excluded from any further analysis. This is to say that any twisting of the wing box would, in principle, translate to a change in the angle of attack of the wing. Additionally, it was considered worth simplifying the process even more by defining a small representative segment of the wing box which will act as a representative structure for the design of the composite laminates. This structure will specifically be used to initially optimize and study how lamination of the spars can affect the response of the wing box. After the laminate designs have been obtained by means of optimization that the short wing box is subjected to, the response using those same laminates of a longer wing box will be evaluated. The longer wing box is not subjected to any optimization under the assumption that no difference would occur in terms of the lamination necessary for the spar to maximize the twist angle, in a qualitative sense. It serves as a direct scale-up case.

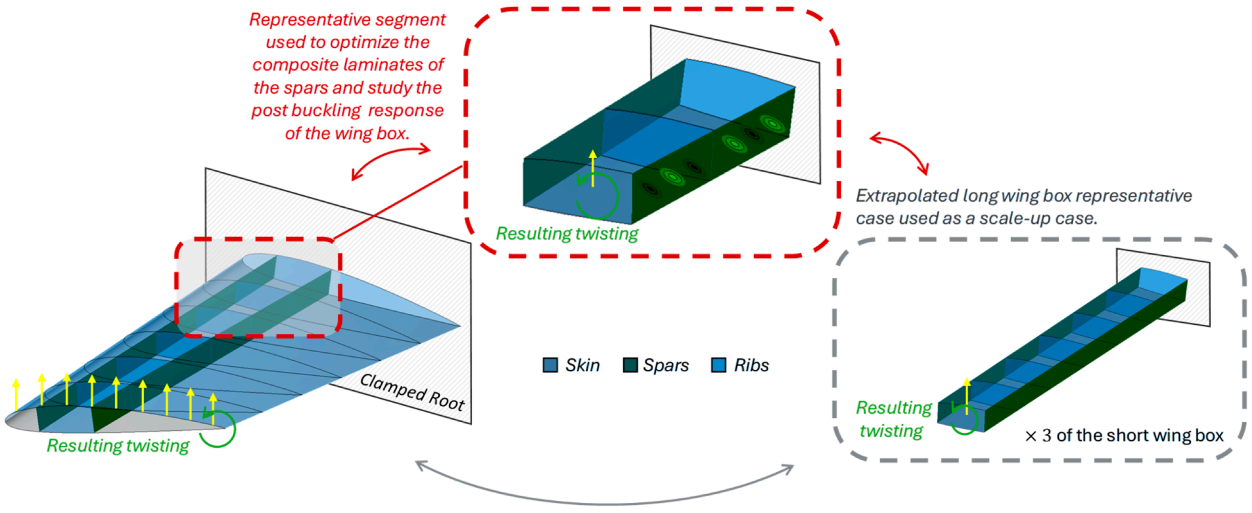


Figure 1. Schematic representation of the overall idea of the simplified representation of the wing box and the interplay between a small representative segment and the larger full-size wing box.

Specifically, it is chosen to work towards optimizing downwards (towards the leading edge) twisting under upwards deflection of the beam (noted by the yellow arrows in Figure 1), and more specifically, maximizing the achievable twist within a certain range of said upwards deflection. The optimization framework is based on the particle swarm optimization (PSO) algorithm in conjunction with finite element analysis (FEA). The optimization framework aids in finding optimal solutions, especially when unconventional angles for the laminate plies of the composite spars are considered. The problem could also be posed in a way where the objective could be targeting a certain twist under a certain deflection, aiming to go towards a more realistic load case, while also considering addi-

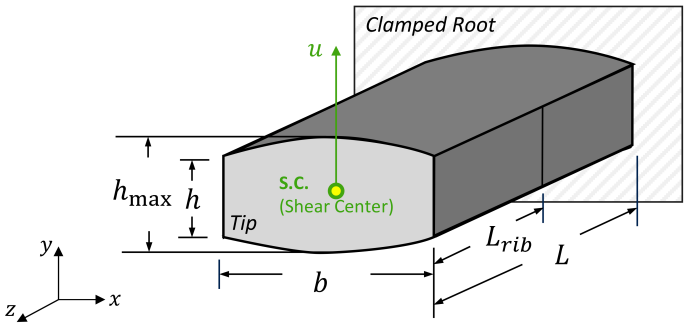
tional constraints and objectives such as achieving a certain critical buckling deflection and above. This would, however, render the problem a multi-objective optimization problem and given that including non-standard angles is already increasing the complexity of the problem to a significant degree, it is avoided. If no consideration of additional constraints is added, then both the maximization and targeted twisting towards a specific value are in effect interchangeable problems. Thus, studying the maximization case is chosen here since it also allows for an evaluation of the extremes.

The more intricate details of the overall model and process are elaborated in the subsections that follow.

2.1. Structural, Geometrical Features and Loading

2.1.1. Geometry and Boundary Conditions

Focusing on the composition and specifics of the representative segment, Figure 2 presents the main geometric characteristics of the short wing box. It is noted that L_{short} refers to the length of the short representative wing box structure, while L_{long} refers to the length of the longer one. The former corresponds to two bays (three ribs including the root), while the latter consists of six bays (seven ribs including the root), which is shown schematically in Figure 1.



h	100 mm
b	250 mm
h_{max}	150 mm
L_{short}	400 mm
L_{long}	1200 mm
L_{rib}	200 mm

Figure 2. Geometry and boundary conditions of the problem of the representative segment of the composite wing box (beam).

At this point, it is noted that the dimensions of the representative structure were rather arbitrarily chosen but are to be in a range that would be normal for a small aircraft in terms of height and width. However, the skin curvature does not follow any specific airfoil shape, but for the sake of simplifying the problem in terms of mechanics, they were both, top and bottom, curved to the height of h_{max} symmetrically using a spline interpolation between the three points. This makes sure the cross section in terms of shape is symmetric about all axes. The boundary conditions consist of an applied deflection at the shear center position at the rib corresponding to the free edge of the beam, while the root is clamped, creating the cantilever conditions. The deflection range is set to 15 mm. For the long wing box case, the deflection range is 95 mm.

2.1.2. Structural Composition

In terms of composition, all components but the ribs are considered to be of IM7/8552 carbon fiber composite laminates the properties of which are reported in Table 1. Both front and rear spars, left and right vertical webs of the beam, are made up of 16-ply laminates while the top and bottom skins are much thicker at 48 plies (Figure 3). This, of course, constitutes the cross section of the wing box at least in terms of thicknesses and overall geometry symmetric with respect to both the horizontal and vertical axes. In terms of lamination, the skin is a $[0, 45, -45, 90]_{6s}$ quasi-isotropic (QI) laminate while the vertical webs are at this point considered of arbitrary lay-up, which is only restricted to being

symmetric and balanced. This is purposefully done as such at this stage since the lay-up of the vertical webs is part of the study and the variable being studied. Indeed, that is what will be optimized later on using the procedure mentioned in the subsequent sections. In a general form, the laminates of the webs are denoted as PAN1 (rear spar, right web) having the lay-up $[\varphi_1, \varphi_2, \varphi_3, \varphi_4, -\varphi_1, -\varphi_2, -\varphi_3, -\varphi_4]_s$ and PAN2 (front spar, left web) $[\varphi_5, \varphi_6, \varphi_7, \varphi_8, -\varphi_5, -\varphi_6, -\varphi_7, -\varphi_8]_s$. Indeed, they are posed in this way to enforce symmetry to the lay-up and the condition that the laminates remain balanced to avoid having the added component of extensional bending coupling in the individual response of the spars contributing to the bending–twisting response of the wing box. It should be understood that for each web, 4 plies are considered independent out of the 16 and will act as the design variables during the optimization later on. For each member, a local material coordinate system is defined, shown in green in Figure 3, to make sure that overall, for every member, the laminate 1 direction (which corresponds to what is the 0° ply longitudinal axis) coincides with the wing box beam axis, while the stacking direction (3 axis) faces outwards.

Table 1. IM7/8552 unidirectional lamina properties [22].

E_{11} (GPa)	E_{22} (GPa)	G_{12} (GPa)	v_{12} (−)
161	11.38	5.2	0.32

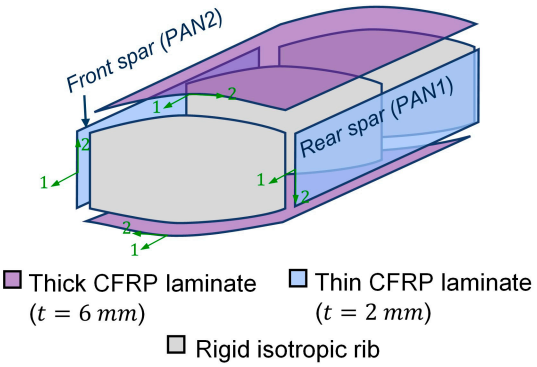


Figure 3. Exploded view of the small representative wing box (beam) segment noting the material composition.

Concerning a few notes on the choices in terms of the laminate thicknesses, what must mainly stand out is the high ply count of the skin. In fact, it was set to this value at this level to, alongside the curved shape of the skins, add onto the overall bending stiffness of the beam to a logical degree, where in post-buckling the skin will not buckle before the spar does or even immediately after. Additionally, this high ply count (48 plies, 6 mm) should also act as a form of a lumped representation of a thinner structure that would also contain stringers (longitudinal stiffening elements). Regarding the spars, the spar thickness set at 16 plies (2 mm) was chosen as such to represent a rather realistic ply count of a potential aircraft spar, which, if thinner, would have a much lower stiffness and thus load-carrying capability before buckling and elasticity of the laminates.

Finally, there was no consideration of different thickness between the vertical webs and this was specifically chosen as such so as to be able to in fact directly determine how the lamination would play into improving, maximizing or tailoring the twisting of the composite beam under bending. An asymmetric distribution of thickness would lead to twisting driven by geometric asymmetry, something that at this point would add one more contributing factor to the kinematic response and was chosen to be avoided in this work to quantify any results occurring purely due to buckling and elastic asymmetry.

2.1.3. Shear Center Position

Now, it has been stated that bending–twisting coupling is to be evaluated and thus it must be ensured that the beam is subjected to bending moments and no torsional moments. To achieve this at least on a theoretical and numerical basis, for a cantilever-like structure like the wing box considered here, it is sufficient to apply the load, in this case deflection, at the shear center of the cross section of the beam. This should induce a linearly increasing bending moment along the length of the beam but no resultant torsional moment. This should hold up until local buckling of one of the spars of the wing box occurs. Thus, any rotations achieved are to be directly attributed to the buckling of the spars. By following the procedure mentioned in Ref. [23] for composite laminates, the position of the shear center can be given by Equation (1). The procedure follows what would be done for isotropic materials but is adjusted for composites by the use of equivalent homogenized properties of the laminates obtained through the classical laminated plate theory (CLPT), which is considered accurate enough as long as the laminates are symmetric and balanced [24,25].

$$x_{sc} = \frac{\left(bh\left(2b\left(A^l_{66}A^r_{66}\left(-E^l_{xx}+E^r_{xx}\right)-6A^l_{66}A^s_{66}E^s_{xx}+6A^r_{66}A^s_{66}E^s_{xx}\right)+A^s_{66}\left(A^r_{66}\left(3E^l_{xx}+E^r_{xx}\right)-A^l_{66}\left(E^l_{xx}+3E^r_{xx}\right)\right)h\right)\right)}{\left(2\left(2A^l_{66}A^r_{66}b+\left(A^l_{66}+A^r_{66}\right)A^s_{66}h\right)\left(6bE^s_{xx}+\left(E^l_{xx}+E^r_{xx}\right)h\right)\right)} \quad (1)$$

where the superscript s, l, r, refers to a quantity that refers to the skin, left and right spar respectively. A_{66} is the (3,3) component of the laminate's A matrix from the ABD matrix of the laminate. E_{xx} is the equivalent elastic modulus of the laminate in the 1 material direction given as $E_{xx} = 1/a_{11}$ where $a_{11} = (A_{22})/(A_{11}A_{22} - (A^2_{12}))$ where A_{11}, A_{22} and A_{12} are the respective components of the A matrix from the ABD matrix of the laminate [26].

In the post-buckled state, which is the most active part of the response looked upon in this study and considered as a continuing useful load-carrying state of the structure, it is noted that it was thought unnecessary to consider the existence of a "shear center". In fact, this has to do with a contradiction with one of the main assumptions present in the theory for defining such cross-sectional properties for beams, namely, a homogeneous and constant cross section along the beam (wing box) axis. Of course, when one of the spars buckles, this assumption is immediately invalidated since along the length of the wing box each individual cross section has a different geometry. So, depending on the position along the beam axis one would choose to look at, the shear center would be rendered at a different location. Nevertheless, it is true that one could intuitively consider and comprehend that there would be a shift in the shear center position in post-buckling because the stiffness of the buckled spar has changed and thus so would the position of the shear center, probably towards the initially less stiff spar. Inevitably, then there would exist a torsional component contingent to this shift in stiffness that would also contribute to the eventual twist of the beam. However, it is considered in this study that it would be part of the overall response attributed to the buckling of the web and, as such, is not decoupled but assumed to be a known contributing factor as to why, after buckling, there is induced twisting.

2.2. The Optimization Framework

It is true that for standard laminates one could perform a manual search and, with some bias due to understanding of composite mechanics, in a rather reasonable time conclude to an optimal solution. However, for the other cases where non-standard angles are also considered as allowable angles for the laminates, the design space grows significantly and to a degree where one could not manually discern a reasonable result with enough certainty. There are many approaches to laminate stacking sequence optimization, depending always on the problem, mainly relying on non-gradient-based methods (e.g., genetic algorithms, Bayesian optimization, PSO, to name a few prominent ones) given the discrete nature of the design variables, which are eventually the ply angles. It is also customary to split

the problem into two steps, where the first step deals with defining the optimal stiffness required for the laminates, usually in the form of invariants or lamination parameters, and the second step deals with the actual angle and, as is typically done in those cases, ply count [27–37].

As stated, the optimization framework used to define the spar laminate lay-ups in this work was built upon the particle swarm optimization (PSO) algorithm [38]. This algorithm is well-established for the optimization of composite lay-ups in various problems of conventional and unconventional angle laminates [27–29,39,40] and is characterized by a simple formulation that is easy to apply, especially in the case of laminates where the ply angles, or bundles of them, are desired to directly be the design variables. Its selection in this work was based on the fact that the relevant literature demonstrates that, as a method, it should be able to easily deal with cases in which permutations of the design variables are considered in a large design space, and it holds a very simplistic logic and implementation, while, as stated in the relevant literature is characterized by good convergence properties.

2.2.1. Particle Swarm Optimization (PSO) Algorithm Basics

While the reader is directed to the original work of Kennedy and Eberhart [38], some basics of the method are noted here. The algorithm is based on the intricate choreography of bird flocks and simulates problems in a way similar to the problem of, for instance, said bird flock finding an optimum feeding ground. The method relies on an initial population of particles, which represent points within the design space (green dots in Figure 4). These particles slowly move within the design space using both personal and societal knowledge of positions that provide better results, always in terms of what they are searching for (the global optimum) and slowly converge all towards that position. Figure 4 schematically shows the process for a two-dimensional problem where the position of the particles is given by a function of the form $f = f(x_1, x_2)$ and the problem is finding the x_1, x_2 combination that minimizes this function. In every iteration of the algorithm, the particles' positions are altered based on the velocity equation, which is given by Equation (2).

$$v = v_0 w + c_1 r_1 \left(P^{best}_{personal} - P_{current} \right) + c_2 r_2 \left(P^{best}_{global} - P_{current} \right) \quad (2)$$

where v is the velocity for each variable of the problem and v_0 the velocity in the previous iteration, w is inertia weight, c_1 is a "personal memory" coefficient and c_2 is a "social information" coefficient, r_1 and r_2 are randomness factors ranging from 0 to 1, $P^{best}_{personal}$ is the personal best position ever held by the particle whose position is being updated, referred to as the personal best position, $P_{current}$, the current position of the particle and P^{best}_{global} is the overall best position held by any particle in the swarm referred to as the global best position. The values of the parameters w, c_1, c_2, are rather important for the method, as they determine how well the particles search the overall design space and how fast they converge to a globally found best position. In the base formulation of the method, w, c_1, c_2 hold constant values. However, in order to search the design space better, it is useful to set it in such a way that it changes along the course of the optimization from a larger to a smaller value [41–43]. In this work, this was included where w starts from an initial value w_{int} and then, after a certain number of iterations at that value, it decreases based on a defined increment, w_{inc}, and so on and so forth. Additionally, what one must be careful of is handling the boundaries of the design space, namely when, during the update of the particle's position, it reaches or surpasses the boundary value [44]. What was implemented in this work was a rerandomization approach where, if the particle reaches the boundary, it is rerandomized to a new position.

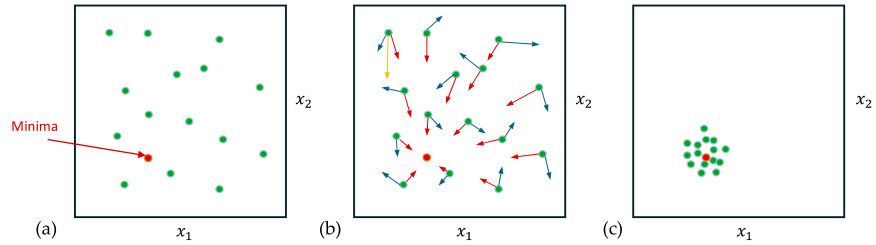


Figure 4. PSO schematic representation of the particle movement in a 2D problem. (**a**) Initial state of the problem and particle positions (**b**) Schematic representation of the velocity (yellow) updates after the first iteration, color coded in total and in social (red) and personal (blue) memory contributions (**c**) Swarm converging to the minima point after some iterations.

2.2.2. Formulation of the Optimization Problem for the Box Beam

In terms of the application of the PSO for the lay-up optimization of the lay-ups of the spars, the problem can be seen as follows. As stated, the objective of the problem is to maximize the achievable twist under bending of the representative simplified wing box segment shown in Figures 2 and 3, which sets the problem as a single-objective maximization problem. Having said that, considering the wing box configuration as shown in Figure 2, the twist of the cross section under loading can be defined based on Equation (3) and as shown in Figure 5. It is noted that the twist will be evaluated by looking at the kinematics of the cross section at the free end of the beam.

$$\theta = \sin^{-1}\left(\frac{u_2^{P2} - u_2^{P1}}{b}\right) \tag{3}$$

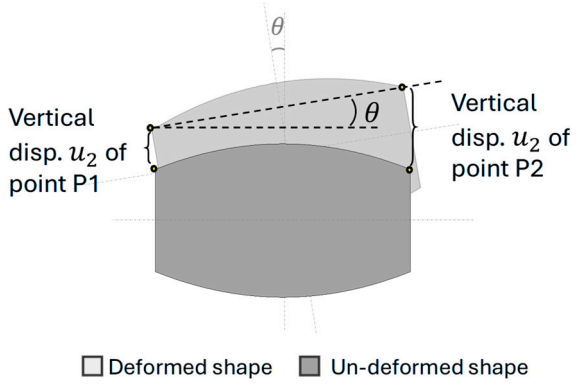


Figure 5. Demonstration of the way the twist angle is calculated based on the wing box (beam) kinematics.

The problem is maximizing $\theta = f(\varphi_1, \varphi_2, \varphi_3, \varphi_4, \varphi_5, \varphi_6, \varphi_7, \varphi_8)$, where it is reminded that the angles φ_k, $k = 1, \ldots, 8$ are the spar laminate independent ply angles noted in Section 2.1.2. These angles are the design variables of the optimization problem as they implicitly affect the kinematics of the wing box and thus the twisting angle achieved, which is the value used in the objective function defined in Equation (4). As is explained in the following section, this was not linked analytically since FEA is used to obtain the resultant kinematics and the twist value. Considering the notation of PAN1 and PAN2 shown in Figure 3, the optimization problem can be defined as:

$$\begin{aligned} &\textit{minimize}: f(\theta) = |\theta_{max} - \theta| \\ &\textit{with the design variables being}: \begin{bmatrix} [\varphi_1, \ldots, \varphi_4, -\varphi_1, \ldots, -\varphi_4]_s \\ [\varphi_5, \ldots, \varphi_8, -\varphi_5, \ldots, -\varphi_8]_s \end{bmatrix} \\ &\textit{subject to}: -\tfrac{90^\circ}{interval} \leq \varphi_k \leq \tfrac{90^\circ}{interval}, \quad k = 1, \ldots, 8 \end{aligned} \tag{4}$$

where φ_k, $k = 1, \ldots, 8$ are the ply angles as explained in Section 2.1.2. θ_{max} is an angle set to a high value which is essentially used to treat the problem of maximization as a minimization problem. Here, the angle $\theta_{max} = 2.29^\circ$ (corresponding to a displacement difference of 10.0 mm between the vertical displacement of points P1 and P2) is used, which is considered a high enough value that no configuration could surpass. The *interval* is what allows the framework to consider unconventional angles. The allowable ply angles are in effect considered to exit in the -90°,90° range with a certain step (e.g., and *interval* = 10° would allow angles like 20°, 30°, 50° but not 55° and 45°). Given the definition of the constraint of φ_k shown in Equation (4), it should be understood that the actual values of the angles φ_k are not degrees but integers in the range $-90^\circ/interval$ and $90^\circ/interval$ (e.g., in the 10° interval case the actual values for φ_k would be the integers in the range -9,9). After defining those, what is used by the FEA in the actual lay-up definition is this value multiplied by the *interval* value. Indeed, this was also done to avoid using the PSO algorithm in a direct discrete variable sense, which is harder to implement and this "*trick*" that sets the design variables as a continuous set of numbers, at least in the integer number set, bypasses that complexity.

On the topic of the number type, it must also be noted that, as mentioned, the mathematics during the PSO algorithm execution, as is done by the explanation in Section 2.2.3. that follows, are done in the set of real numbers. This does conflict with the purely integer nature of the design variables. To circumvent that, after each update of the position of the particle, which is done by Equation (2) per variable, the value of the new position the variable obtains is rounded up or down to the nearest integer. Given that the variables are defined in a continuous manner in the integer number space, this is not considered detrimental to the accuracy of the algorithm's implementation and thus its functionality.

2.2.3. Implementation

Some of the decisions mentioned above also had to deal with the fact that this framework was to be integrated with Abaqus [45] using Abaqus/Standard and Python scripting capabilities.

The framework is implemented using a single Python script. The script starts by initializing the design variables to their initial random values for a certain number of particles. Then this feeds an analysis loop where, for every particle, the respective simulation of the simplified wing box is executed. In fact, for each particle, before the FEA simulation is submitted, first the position of the shear center is calculated and the load application point (reference point) is altered based on Equation (2) while the lay-ups are also altered accordingly to the particle's specifications. After the simulation runs, the results are postprocessed to provide the value of the objective function, i.e., angle of twist, per particle, which is saved. Upon exiting the loop, the actual PSO part of the procedure is run where global and personal best positions are found and updated and eventually the particles move to their new positions for the next iteration. This interchange between the FEA and PSO loops is repeated for a predefined number of iterations, which serves as the loop termination criterion. At the end, the particle holding the global best position is noted as the optimized solution. Ideally, what would also be seen is all particles having converged to this position. Figure 6 provides a schematic representation of the flow chart of the framework.

The Finite Element Analysis (FEA) Model

The model consists of the wing box defined using conventional reduced integration shell elements (S4R) with a universal average size of 3 mm $\times$ 3 mm, selected after a mesh convergence study was performed. All the ribs but the one sitting at the tip are modeled using a central reference point in the plane of the rib that is connected to the respective

cross-sectional nodes via a beam type MPC. For the tip, the reference point is positioned at the location of the shear center and connected to the rib edge nodes via a rigid body (node based) connection. The meshing scheme and rib representation are kept the same for both the short representative structure of a 0.4 m length and the long one of a length of 1.2 m. The solver used is the nonlinear static solver with automatic stabilization, with a dissipated energy factor of 1.0×10^{-8}. All other solution parameters are kept to their defaults.

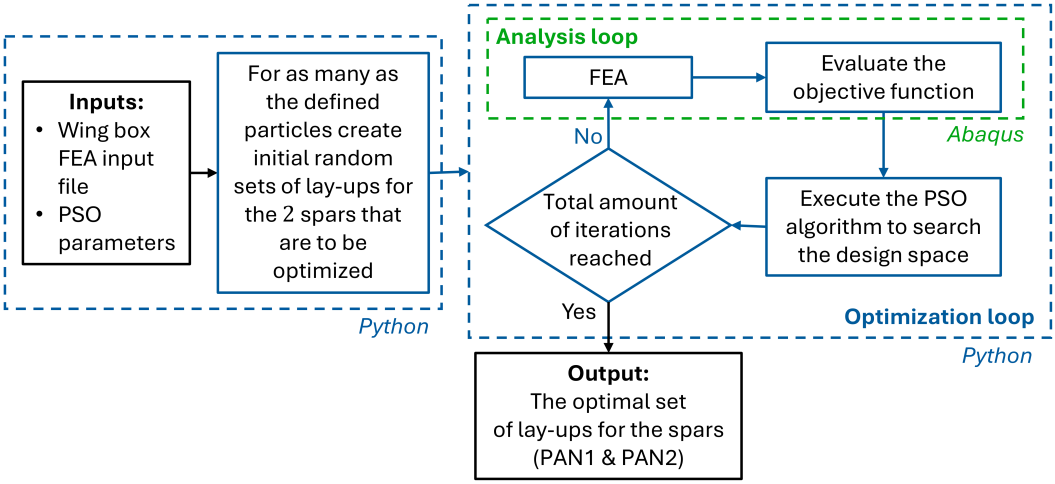


Figure 6. Descriptive flow chart of the optimization framework.

3. Case Studies and Results

The objective is to maximize the twist angle the wing box sustains due to buckling of the spar in a downward fashion under upward deflection, and as mentioned, the distinctive feature over which different solutions are sought is the allowable range of ply angles. Three cases of angle intervals are considered: 45°, 15° and 5°. The first case represents a classical quad-based lamination approach having an interval of 45°, allowing 0°, 90°, ±45° as possible ply angles. The 15° interval case leads to the allowable angles, 0°, ±15°, ±30°, ±45°, ±60°, ±75°, 90° and for the 5° interval case those are 0°, ±5°, ±10°, ±15°, ±20°, ±25°, ±30°, ±35°, ±40°, ±45°, ±50°, ±55°, ±60°, ±65°, ±70°, ±75°, ±80°, ±85°, 90°.

To attain a sense of the size of the problems studied, using the theory of permutations with repetitions, the total number of possible arrangements per case to be considered can be defined. Remembering that for the problem studied here each panel has four independent ply angles that will be optimized (combined and evaluated upon resulting twist) it can be found that for the 45° interval case, where the possible values of the four plies are four, the possible arrangements are 256 (4^4). The 15° interval allows 12 discrete values for the 4 plies, which leads to a possible 20,736 (12^4) arrangements per spar, and then for the 5° interval case, where the independent possible angles are 36, this leads to 1,679,616 (36^4) possible arrangements per spar. This should demonstrate how large the problem easily becomes when the lamination is subjected to a wider range of allowable ply angles, especially if one considers that there would also be a combination of possible laminate arrangements for the wing box problem, which contains two spars. Looking at these numbers is important in order to understand how the parameters of the PSO algorithm used should be chosen per case. While a formal optimization of the PSO parameters themselves is not done, the movement of the swarm in the design space was observed after several runs of the optimization algorithm to conclude the final PSO parameters used to obtain the presented results, which are reported in Table 2 for each case. The number of particles used is capped by the available computational resources to the authors.

Table 2. PSO parameters used per studied case.

	45° Interval	**15° Interval**	**5° Interval**
Number of particles	16	72	72
w_{int}	1.2	2.0	3.0
w_{inc}	0.2	0.2	0.2
c_1	0.7	0.7	0.7
c_2	0.8	0.8	0.8
Iterations per w_{inc}	4	4	6
Total iterations	20	40	90

It is noted that, given the size of the design space, the choice of PSO parameters that also considered the computational resources available to the authors, and the propensity of the PSO algorithm to converge to local minima [43], more than one run of the optimization algorithm was subjected to the same parameters, for the 15° and 5° interval cases, which are the large problems. However, only one result is reported per case, which was chosen as the best between the runs, i.e., manually checking the optimal one of the local minima the PSO algorithm reached for those cases. Table 3 reports the results showing the lay-ups per spar and useful related measures, namely, equivalent laminate moduli, E_{xx}, E_{yy}, G_{xy} calculated using classical laminated plate theory, shear center position along the x-axis, critical buckling deflection and the rotation achieved for the short and long wing box configurations.

Table 3. Overview of the PSO results per studied case.

	45° Interval	**15° Interval**	**5° Interval**
PAN1 $[\varphi_1, \varphi_2, \varphi_3, \varphi_4]$	$[-45, 45, 45, -45]$	$[45, 30, 60, 45]$	$[55, 60, 50, 60]$
E_{xx}(GPa)	18.66	32.08	14.03
E_{yy}(GPa)	18.66	32.08	42.87
G_{xy}(GPa)	41.58	37.03	35.69
PAN2 $[\varphi_5, \varphi_6, \varphi_7, \varphi_8]$	$[0, 0, 0, 0]$	$[0, 15, -15, 90]$	$[0, 40, -90, -65]$
E_{xx}(GPa)	161.00	113.54	59.92
E_{yy}(GPa)	11.38	49.05	70.31
G_{xy}(GPa)	5.20	9.75	17.68
Shear center position (mm)	149.28	95.09	74.19
Critical buckling deflection (mm)	3.89	2.08	2.65
Max rotation (small wing box)	0.85°	0.72°	0.57°
Max rotation (long wing box)	1.46°	1.21°	0.78°

In terms of looking at the evolution of the kinematics of the wing box during loading, considering pre-buckling, transition to buckling and the post-buckling regime, Figure 7 demonstrates the vertical reaction force at the clamp over the deflection for each case regarding the short beam analysis, which are the results of the optimization runs. The figures show the force-deflection curve alongside images of the contour plot (the rainbow follows the typical convention in Abaqus where red refers to the maximum value and blue to the minimum) of the out-of-plane displacement immediately after the critical buckling deflection, and the displacement magnitude at 12 mm of applied deflection representing a post-buckling state. In these figures, it is clearly seen that buckling is characterized by a local buckling mode restricted to the rear spar, signified by the change in stiffness. In the 45° and 15° interval cases, this is not accompanied by any buckling of the front spar within

the range considered (i.e., deflections of up to 15 mm). In those cases, this corresponds to a bi-stable condition and solution for the 15 mm applied deflection range. However, for the 5° interval case within this loading range, there are two local buckling events, first the rear spar and then the front spar, leading to an eventual multi-stable response for the short wing box. Considering the observed buckling mode in the 45° and 15° interval cases, two half-waves develop per bay in the rear spar and three half-waves for the 5° interval case.

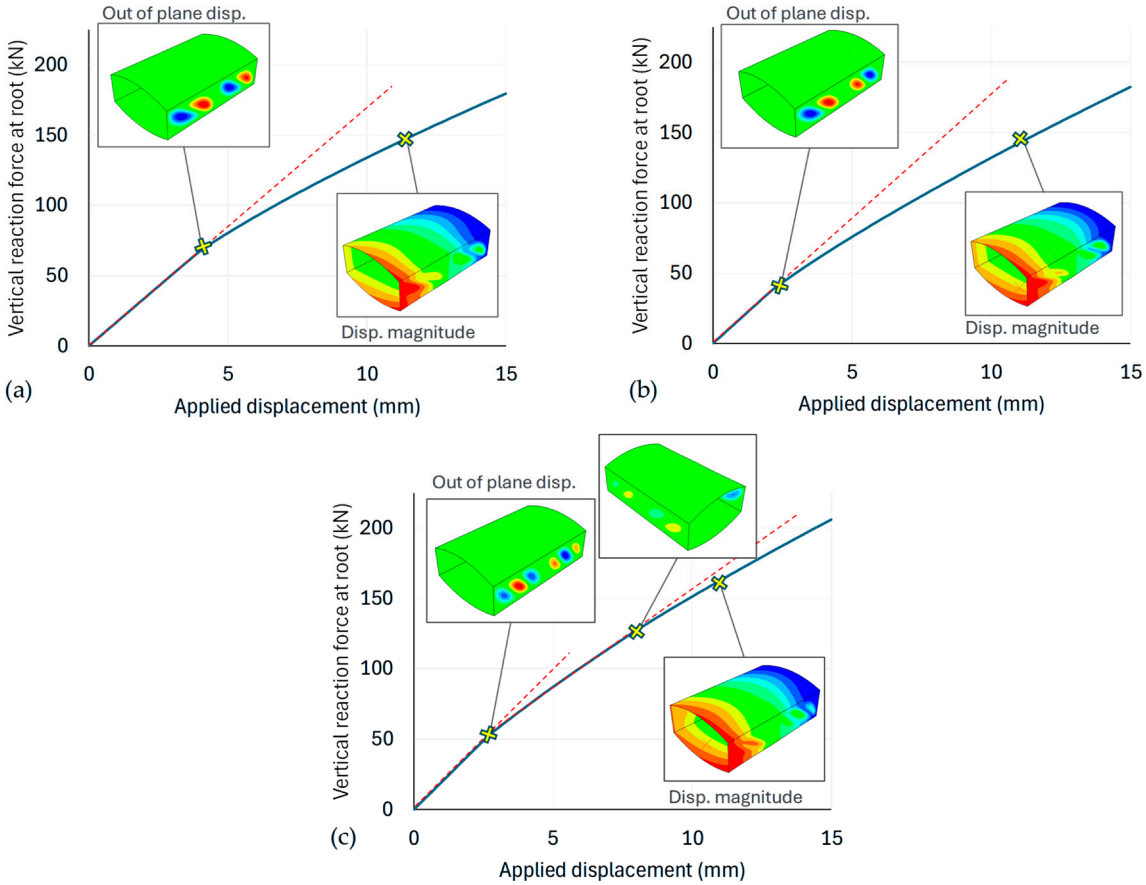


Figure 7. Vertical reaction force vs. applied displacement plots for the studied cases of the small representative segment: (**a**) 45° interval, (**b**) 15° interval, (**c**) 5° interval. The images show the displacements, i.e., kinematics of the wing box at certain time steps and the red dashed line represents the linear solution.

As mentioned, these laminates were also used to evaluate the response of the long wing box. The results for those cases in terms of reaction force over applied deflection are shown in Figure 8. It is noted that for this configuration, none of the cases led to buckling of the front spar before reaching the full range of loading applied, which is 95 mm. Again, the force deflection plot is accompanied by an image of the out-of-plane displacement, focusing on the rear spar, at 80 mm applied deflection, showing a state in the post-buckling stage of loading. The buckling mode here follows the same pattern as that obtained for the short beam, characterized by two half waves per bay of the rear spar for the 45° and 15° interval cases and three half waves for the 5° interval case.

More importantly, the respective evolution of the tip twist angle during loading is given in Figure 9 for both the short and long wing boxes, respectively, and compared per case. Based on these results and the results reported in Table 3, what can be understood is that the case for the 45° interval renders the best overall result in terms of a maximized twisting angle. The other two cases lie slightly lower but always within a range of 0.2°

difference for the short case and 0.8° difference for the long case, rendering them, however, fairly similar in magnitude.

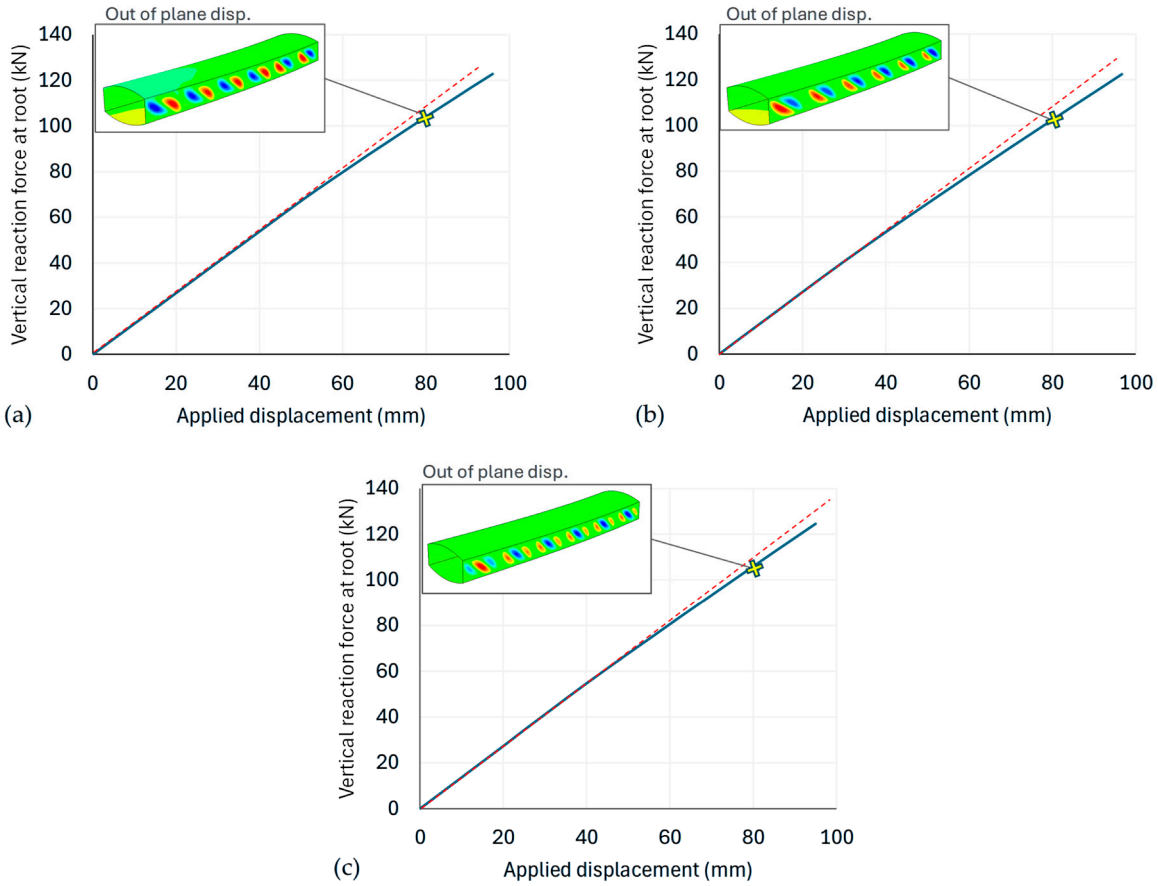


Figure 8. Vertical reaction force vs. applied displacement plots for the studied cases of the long wing box at 1.2 m length: (**a**) 45° interval, (**b**) 15° interval, (**c**) 5° interval. The images show the displacements, i.e., kinematics of the wing box at certain time steps and the red dashed line represents the linear solution.

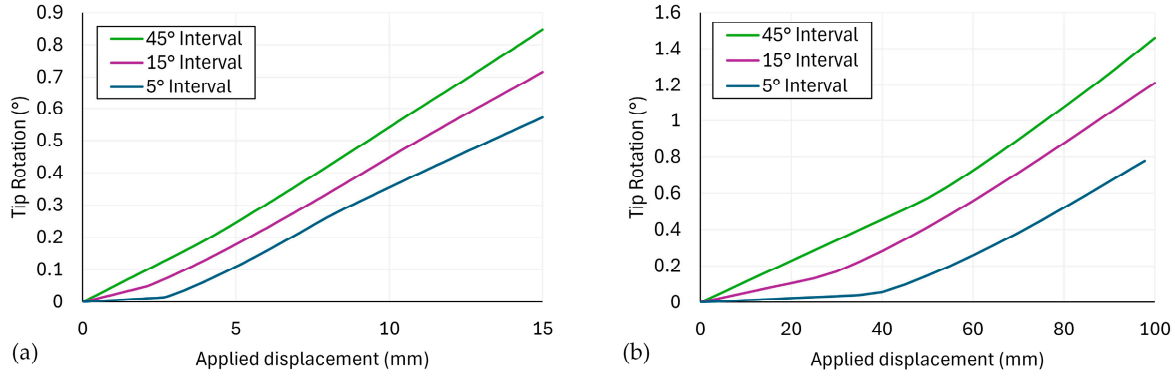


Figure 9. Rotation achieved at the free end of the wing box for (**a**) the small representative segment and (**b**) the long wing box.

Seemingly contrary to what was discussed in Section 2.1.2., it can be seen that for the 45° interval case especially and the 15° interval case, there is an appreciable twisting component even before buckling occurs. To the best of the authors' knowledge, this can be attributed to the fact that despite the best of efforts, the calculated shear center might not be a "*true*" shear center in the classical sense pertaining to isotropic materials. In fact,

as stated in Ref. [25] with composite laminated beams the calculation of a shear center might be an ambiguous thing as inherent elastic couplings in the response of composite laminates cannot in totality guarantee that applying a no twist condition, basic condition for the shear center calculation can guarantee a zero-twisting moment, and vice versa, even though concluding that in principle the theory should be in ways extendable to the case of balanced and symmetric laminated webs.

In fact, for the 45° case, the shear center, based on Equation (1), is calculated to lie outside the cross section, something that for a closed section does not intuitively seem valid. Looking at the shear moduli of PAN1 and PAN2 alone, it is evident that there is a significant discrepancy in magnitude between the two, with a ratio between right and left spars of $G^r_{xy}/G^l_{xy} = 8.0$. This signifies that for this geometric configuration, the front spar is essentially equivalent to a very thin or non-existent web in the beam due to its severely lower shear stiffness value, also rendering the beam itself highly anisotropic. This combination of spar laminates is understood, though, to be the extreme case. On the contrary, the laminates achieved for the 15° and 5° cases are less orthotropic on their own and are closer to each other in terms of shear stiffness, namely $G^r_{xy}/G^l_{xy} = 3.8$ and $G^r_{xy}/G^l_{xy} = 2.0$, rendering the overall cross section of the wing box intuitively less anisotropic, with some inevitable loss in achieved rotational magnitude. Hence, the 45° case also heavily relies on the elastic anisotropy of the cross section to provide the highest overall twist angle.

To additionally get a different perspective on the obtained results, what was also evaluated was the rate of change in rotation angle to better decouple the two phases of loading, namely pre and post-buckling. The rates were normalized based on the minimum, representing the rate of twist existing in the linear pre-buckling range for each case, and are depicted in Figure 10 that follows.

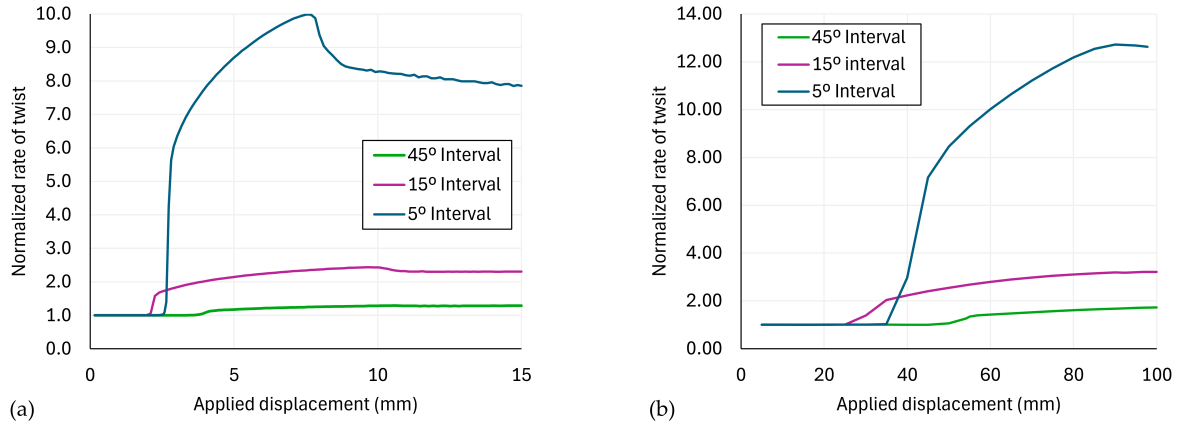


Figure 10. Rate of rotation with respect to applied displacement at the free end of the wing box for (**a**) the small representative segment and (**b**) the long wing box.

Contrary to the previous observations based on total rotational value, looking at the rate of rotation does demonstrate that the 5° interval case provides the highest effect in post-buckling. Interestingly, while for the 45° interval case the rate of rotation increases only by 1.5 times the pre-buckling rate in post-buckling, for the 15° interval case it is increased by 3 times and even more significantly by 10 times for the 5° interval case. This demonstrates that while the overall rotation is comparable, the actual contribution due to buckling using an unconventional lay-up can have significant gains.

Discussion

In terms of overall optimal solution, always considering the maximization of the twisting under bending, it should be evident that the best solution lies in the result obtained

for the 45° interval case. This means a ±45° laminate for the rear spar and a UD 0° laminate for the front spar. This is attributed indeed to the fact that these laminates present the extrema in terms of lamination pertaining mainly to shear stiffness maximum and minimum achievable values for a laminate. What this does point out is the fact that for any such wing box, namely a rectangular cross-sectional configuration, this combination of lateral spar laminates would and does provide the twist angle maximum range within which a designer could later on proceed to try to tailor the buckling induced twisting.

Now, concerning the optimization itself, while the ±45° and UD laminate combination so far seems to be the best (i.e., the global optimum), and is still an allowable solution also for the laminates that are being optimized with the 15° and 5° intervals, the PSO algorithm did not converge to that solution in those cases. This would, of course, depend on the parameters and the number of particles considered for the runs, which, as aforementioned, is not fully explored in this work due to resource restrictions. While a combination of lay-ups that would lead to similar or close enough stiffness towards the ±45° and UD results could potentially be found using a different set of 15° and 5° ply angle based lay-ups, the solutions provided for the number of iterations run are still considered representative, even though they are local minima. This holds especially when considering the study aimed at qualitatively assessing the benefits achievable for such problems when using unconventional angles. Along those lines, the differences and results reported found with the runs executed for this study were considered sufficient to this extent.

Going back to evaluating the laminates in terms of the set objective, namely maximizing twist angle under bending, while the overall angle of rotation might be slightly lower for the unconventional laminates, they do present some unique advantages as observed by the results presented in this study. One of those being the fact that the cross section itself is less anisotropic. Indeed, the design provided with a UD and a ±45° laminate is also not necessarily realistic since, especially considering the purely UD laminate, it would rarely be used in an actual aircraft wing where more complex multiaxial loading cases also need to be considered. So, the results provided for the 15° and 5° interval cases hold more realistic potential for a general use case.

Alongside this, as observed using an unconventional lay-up, namely the lay-up achieved for the 5° case, allows for a significant change in overall bending–twisting coupling response between the pre-buckling and post-buckling state. In fact, with this design leading to a 10 times increase in the rate of twist, does hint to the fact that it is expected to indeed have much higher potential and room to explore in terms of design versatility.

Additionally, a most interesting observation and result can be seen in the response of the 5° interval solution. The laminate combination the optimization landed on demonstrates a multi-stable response with sequential buckling of the two spars within the range of 15 mm applied deflection, which is the same used for all cases. While it cannot be fully known if similar trends could be observed using typical quads under an objective that mainly focuses on for instance optimizing post buckling rotation rate, which here was not the case, it certainly does concur the fact that expanding the design space in such a way can certainly give more control over the design and higher overall flexibility in terms of potential constraints future works could implement to perform more complex studies related to adaptive wing structures subjected to a more multi-objective case study, e.g., maximizing overall twisting under bending and multi-stability. In fact, better understanding the driving mechanisms for this would be imperative. The discussion in this text mainly focused on the shear stiffness as a driving factor for explaining and understanding the observed responses. Intuitively, it can be seen that both spars enter buckling within the selected loading range when their shear stiffnesses are closer to each other, presenting a lower overall ratio G^r_{xy}/G^l_{xy}. However it is noted that, since especially in the post-buckling

state, when considering that the webs are not of an isotropic nature but rather laminated composites whose buckling response does mainly depend on the bending stiffnesses the laminate has [46], it is hard to directly make a definitive statement on the effect the shear stiffness ratio could have on this when regarding the wing box structure. Qualitatively, it seems so, but to more concretely conclude towards something in terms of explaining this, a much more exhaustive study would have to be performed, and it was not considered part of this study at this point.

4. Conclusions

On the subject of achieving an adaptive composite wing structure driven by buckling, the specific response of a composite wing box under bending–twisting coupling was studied, aiming at expanding the overall understanding of the mechanics of such buckling-driven adaptive designs. More specifically, the potential of the use of unconventional angles in the laminates of the spars to optimize the response of the wing box was investigated.

It was shown that the maximum coupling can be achieved relying on the use of standard angles, namely a UD and a $\pm 45^{\circ}$ angled ply laminate. However, that result does rely on a highly anisotropic cross section design that would hinder its actual use in a realistic case where a more multiaxial loading state is to be expected. Thus, the designs provided relying on both 15° and 5° intervals of potential ply angles seem to produce comparable twisting while holding a less anisotropic composition. In fact, the large design space in the latter case, as the results demonstrated, also allows for multi-stability to be considered with more ease while accommodating a stronger buckling-driven twisting response evident by the differences obtained in rates of post-buckling rotations.

As a consequence, it is considered that the use of unconventional laminates is recommended to achieve tailored adaptive capabilities, especially considering them stemming from the buckling response of the structures themselves. Indeed, that was why this work focused on utilizing lamination to affect the bending–twisting response solely, in order to decouple any results from the use of geometric asymmetries or elastic coupling, which would also affect the outcome. Future work will focus on achieving tailored multi-stability and, in fact, building and testing some of these designs to assess just how reliant the analysis is, especially when considering the utilization of buckling in design.

Author Contributions: A.M.: Conceptualization, methodology, software, formal analysis, writing—original draft preparation. C.B.: Conceptualization, funding, resources, supervision, writing—review and editing. All authors have read and agreed to the published version of the manuscript.

Funding: Funded by the European Union (ERC Advanced Grant, NABUCCO, project number 101053309). Views and opinions expressed are however those of the authors only and do not necessarily reflect those of the European Union or the European Research Council Executive Agency. Neither the European Union nor the granting authority can be held responsible for them.

Data Availability Statement: Data available in a publicly accessible repository at the link: https://doi.org/10.5281/zenodo.21373898.

Conflicts of Interest: The authors declare no conflicts of interest.

References

1. Weisshaar, T.A. Morphing Aircraft Systems: Historical Perspectives and Future Challenges. *J. Aircr.* **2013**, *50*, 337–353. [CrossRef]
2. Ajaj, R.M.; Saavedra Flores, E.I.; Friswell, M.I.; Allegri, G.; Woods, B.K.S.; Isikveren, A.T.; Dettmer, W.G. The Zigzag Wingbox for a Span Morphing Wing. *Aerosp. Sci. Technol.* **2013**, *28*, 364–375. [CrossRef]
3. Xia, Y.; Huang, G.; Dai, Y.; Yang, C. Enhanced Aerodynamic Performance of Wings by Spanwise Morphing: Insights from Force Partitioning. *AIAA J.* **2025**, *63*, 4818–4835. [CrossRef]

4. Zhang, J.; Bisagni, C. Buckling-Driven Mechanisms for Twisting Control in Adaptive Composite Wings. *Aerosp. Sci. Technol.* **2021**, *118*, 107006. [CrossRef]
5. Bishay, P.L.; Burg, E.; Akinwunmi, A.; Phan, R.; Sepulveda, K. Development of a New Span-Morphing Wing Core Design. *Designs* **2019**, *3*, 12. [CrossRef]
6. Kota, S.; Hetrick, J.; Osborn, R.; Paul, D.; Pendleton, E.; Flick, P.; Tilmann, C. Design and Application of Compliant Mechanisms for Morphing Aircraft Structures. In *Proceedings of the Smart Structures and Materials 2003: Industrial and Commercial Applications of Smart Structures Technologies*; Anderson, E.H., Ed.; SPIE: Bellingham, WA, USA, 2003.
7. Runkel, F.; Fasel, U.; Molinari, G.; Arrieta, A.F.; Ermanni, P. Wing Twisting by Elastic Instability: A Purely Passive Approach. *Compos. Struct.* **2018**, *206*, 750–761. [CrossRef]
8. De Gaspari, A.; Riccobene, L.; Ricci, S. Design, Manufacturing and Wind Tunnel Validation of a Morphing Compliant Wing. *J. Aircr.* **2018**, *55*, 2313–2326. [CrossRef]
9. Rivero, A.E.; Weaver, P.M.; Cooper, J.E.; Woods, B.K.S. Structural Modeling of Compliance-Based Camber Morphing Structures Under Transverse Shear Loading. *AIAA J.* **2020**, *58*, 4941–4951. [CrossRef]
10. Vos, R.; Gürdal, Z.; Abdalla, M. Mechanism for Warp-Controlled Twist of a Morphing Wing. *J. Aircr.* **2010**, *47*, 450–457. [CrossRef]
11. Arrieta, A.F.; Kuder, I.K.; Rist, M.; Waeber, T.; Ermanni, P. Passive Load Alleviation Aerofoil Concept with Variable Stiffness Multi-Stable Composites. *Compos. Struct.* **2014**, *116*, 235–242. [CrossRef]
12. Pabon, J.A.; Gao, X.; Cai, J.; Gunasekaran, S. Experimental Investigation of a Novel Morphing Wing Design. In *Proceedings of the AIAA SCITECH 2024 Forum*; American Institute of Aeronautics and Astronautics: Reston, VA, USA, 2024.
13. Auteri, F.; Savino, A.; Zanotti, A.; Gibertini, G.; Zagaglia, D.; Bmegaptche Tekap, Y.; Braza, M. Experimental Evaluation of the Aerodynamic Performance of a Large-Scale High-Lift Morphing Wing. *Aerosp. Sci. Technol.* **2022**, *124*, 107515. [CrossRef]
14. Servetti, G.; Cestino, E.; Frulla, G. Parametric Evaluation of Morphed Wing Effectiveness. *Aerospace* **2026**, *13*, 187. [CrossRef]
15. Thuwis, G.A.A.; De Breuker, R.; Abdalla, M.M.; Gürdal, Z. Aeroelastic Tailoring Using Lamination Parameters. *Struct. Multidiscip. Optim.* **2010**, *41*, 637–646. [CrossRef]
16. Xie, H.; Zhang, S.; Yang, Y.; Zhou, Y.; Zhao, H. Design of Variable-Stiffness Bistable Composite Laminates and Their Application in Variable-Camber Wings. *Aerospace* **2025**, *12*, 525. [CrossRef]
17. Serafeim, G.P.; Manolas, D.I.; Riziotis, V.A.; Chaviaropoulos, P.K.; Saravanos, D.A. Optimized Blade Mass Reduction of a 10MW-Scale Wind Turbine via Combined Application of Passive Control Techniques Based on Flap-Edge and Bend-Twist Coupling Effects. *J. Wind Eng. Ind. Aerodyn.* **2022**, *225*, 105002. [CrossRef]
18. Piatak, D.J.; Nixon, M.W.; Kosmatka, J.B. *Stiffness Characteristics of Composite Rotor Blades with Elastic Couplings*; NASA-TP-3641; NASA Langley Technical Report Server: Hampton, VA, USA, 1997.
19. Marano, A.D.; Belardo, M.; Beretta, J.; Starace, F.; Orlando, S.; Punzi, C.; Frajese, R.; Paletta, N.; Di Palma, L. Aeroelastic Tailoring of the Next Generation Civil Tiltrotor Technological Demonstrator Composite Wing. *Aerospace* **2022**, *9*, 335. [CrossRef]
20. Vanegas-Alzate, J.P.; Restrepo-Madrigal, M.A.; Torres-Madroñero, J.L.; Nieto-Londoño, C.; Barragán de los Rios, G.A.; Tamayo-Avendaño, J.M.; Sierra-Pérez, J.; Alvarez-Montoya, J.; Restrepo-Montoya, D. Bend–Twist Coupling for Small Wind Turbines: A Blade Design Methodology to Enhance Power Generation. *Energies* **2025**, *18*, 5353. [CrossRef]
21. Papadakis, N.; Condaxakis, C. An Experimental Performance Assessment of a Passively Controlled Wind Turbine Blade Concept: Part A—Isotropic Materials. *Energies* **2024**, *17*, 3049. [CrossRef]
22. Krueger, R. A Summary of Benchmark Examples to Assess the Performance of Quasi-Static Delamination Propagation Prediction Capabilities in Finite Element Codes. *J. Compos. Mater.* **2015**, *49*, 3297–3316. [CrossRef]
23. Megson, T.H.G. *Aircraft Structures for Engineering Students*; Elsevier: Amsterdam, The Netherlands, 2022.
24. Kollar, L.P.; Pluzsik, A. Analysis of Thin-Walled Composite Beams with Arbitrary Layup. *J. Reinf. Plast. Compos.* **2002**, *21*, 1423–1465. [CrossRef]
25. Pollock, G.D.; Zak, A.R.; Hilton, H.H.; Ahmad, M.F. Shear Center for Elastic Thin-Walled Composite Beams. *Struct. Eng. Mech.* **1995**, *3*, 91–103. [CrossRef]
26. Nettles, A.T. *Basic Mechanics of Laminated Composite Plates*; NASA-RP-1351; NASA Langley Technical Report Server: Hampton, VA, USA, 1994.
27. Pitton, S.F.; Ricci, S.; Bisagni, C. Buckling Optimization of Variable Stiffness Cylindrical Shells through Artificial Intelligence Techniques. *Compos. Struct.* **2019**, *230*, 111513. [CrossRef]
28. Suresh, S.; Sujit, P.B.; Rao, A.K. Particle Swarm Optimization Approach for Multi-Objective Composite Box-Beam Design. *Compos. Struct.* **2007**, *81*, 598–605. [CrossRef]
29. Bloomfield, M.; Herencia, J.; Weaver, P. Optimisation of Anisotropic Composite Plates Incorporating Non-Conventional Ply Orientations. In *Proceedings of the 49th AIAA/ASME/ASCE/AHS/ASC Structures, Structural Dynamics, and Materials Conference, 16th AIAA/ASME/AHS Adaptive Structures Conference*; American Institute of Aeronautics and Astronautics: Reston, VA, USA, 2008.
30. Ntourmas, G.; Glock, F.; Deinert, S.; Daoud, F.; Schuhmacher, G.; Chronopoulos, D.; Özcan, E.; Ninić, J. Stacking Sequence Optimisation of an Aircraft Wing Skin. *Struct. Multidiscip. Optim.* **2023**, *66*, 31. [CrossRef]

31. Bisagni, C.; Lanzi, L. Post-Buckling Optimisation of Composite Stiffened Panels Using Neural Networks. *Compos. Struct.* **2002**, *58*, 237–247. [CrossRef]
32. Chen, S.; Lin, Z.; An, H.; Huang, H.; Kong, C. Stacking Sequence Optimization with Genetic Algorithm Using a Two-Level Approximation. *Struct. Multidiscip. Optim.* **2013**, *48*, 795–805. [CrossRef]
33. Albazzan, M.A.; Harik, R.; Tatting, B.F.; Gürdal, Z. Efficient Design Optimization of Nonconventional Laminated Composites Using Lamination Parameters: A State of the Art. *Compos. Struct.* **2019**, *209*, 362–374. [CrossRef]
34. Bisagni, C.; Vescovini, R. Fast Tool for Buckling Analysis and Optimization of Stiffened Panels. *J. Aircr.* **2009**, *46*, 2041–2053. [CrossRef]
35. Montemurro, M.; Fiordilino, G.A.; Carrera, E. Multi-Level Optimisation of Composite Structures through a Global-Local Modelling Approach Based on High-Order Theories. *Comput. Struct.* **2023**, *275*, 106932. [CrossRef]
36. Chuaqui, T.R.C.; Rhead, A.T.; Butler, R.; Scarth, C. A Data-Driven Bayesian Optimisation Framework for the Design and Stacking Sequence Selection of Increased Notched Strength Laminates. *Compos. B Eng.* **2021**, *226*, 109347. [CrossRef]
37. Zehnder, N.; Ermanni, P. A Methodology for the Global Optimization of Laminated Composite Structures. *Compos. Struct.* **2006**, *72*, 311–320. [CrossRef]
38. Kennedy, J.; Eberhart, R. Particle Swarm Optimization. In *Proceedings of the ICNN'95—International Conference on Neural Networks*; IEEE: New York, NY, USA, 1995; pp. 1942–1948.
39. Chang, N.; Wang, W.; Yang, W.; Wang, J. Ply Stacking Sequence Optimization of Composite Laminate by Permutation Discrete Particle Swarm Optimization. *Struct. Multidiscip. Optim.* **2010**, *41*, 179–187. [CrossRef]
40. Rao, A.R.M.; Lakshmi, K. Discrete Hybrid PSO Algorithm for Design of Laminate Composites with Multiple Objectives. *J. Reinf. Plast. Compos.* **2011**, *30*, 1703–1727. [CrossRef]
41. Shi, Y.; Eberhart, R.C. Empirical Study of Particle Swarm Optimization. In *Proceedings of 1999 Congress on Evolutionary Computation-CEC99 (Cat. No. 99TH8406)*; IEEE: New York, NY, USA, 1999; pp. 1945–1950.
42. Arasomwan, M.A.; Adewumi, A.O. On the Performance of Linear Decreasing Inertia Weight Particle Swarm Optimization for Global Optimization. *Sci. World J.* **2013**, *2013*, 860289. [CrossRef]
43. Schmitt, M.; Wanka, R. Particle Swarm Optimization Almost Surely Finds Local Optima. *Theor. Comput. Sci.* **2015**, *561*, 57–72. [CrossRef]
44. Chu, W.; Gao, X.; Sorooshian, S. Handling Boundary Constraints for Particle Swarm Optimization in High-Dimensional Search Space. *Inf. Sci.* **2011**, *181*, 4569–4581. [CrossRef]
45. Dassault Systèmes SIMULIA Corp. *Abaqus 2024 Analysis User's Guide*; Dassault Systèmes SIMULIA Corp.: Providence, RI, USA, 2024.
46. Reddy, J.N. *Mechanics of Laminated Composite Plates and Shells*; CRC Press: Boca Raton, FL, USA, 2003.

Disclaimer/Publisher's Note: The statements, opinions and data contained in all publications are solely those of the individual author(s) and contributor(s) and not of MDPI and/or the editor(s). MDPI and/or the editor(s) disclaim responsibility for any injury to people or property resulting from any ideas, methods, instructions or products referred to in the content.